

Concentration bounds for linear Monge mapping estimation and optimal transport domain adaptation

Rémi Flamary*, Karim Lounici*, André Ferrari

August 27, 2021

Abstract

This article investigates the quality of the estimator of the linear Monge mapping between distributions. We provide the first concentration result on the linear mapping operator and prove a sample complexity of $n^{-1/2}$ when using empirical estimates of first and second order moments. This result is then used to derive a generalization bound for domain adaptation with optimal transport. As a consequence, this method approaches the performance of theoretical Bayes predictor under mild conditions on the covariance structure of the problem. We also discuss the computational complexity of the linear mapping estimation and show that when the source and target are stationary the mapping is a convolution that can be estimated very efficiently using fast Fourier transforms. Numerical experiments reproduce the behavior of the proven bounds on simulated and real data for mapping estimation and domain adaptation on images.

Abstract

This article investigates the quality of the estimator of the linear Monge mapping between distributions. We provide the first concentration result on the linear mapping operator and prove a sample complexity of $n^{-1/2}$ when using empirical estimates of first and second order moments. This result is then used to derive a generalization bound for domain adaptation with optimal transport. As a consequence, this method approaches the performance of theoretical Bayes predictor under mild conditions on the covariance structure of the problem. We also discuss the computational complexity of the linear mapping estimation and show that when the source and target are stationary the mapping is a convolution that can be estimated very efficiently using fast Fourier transforms. Numerical experiments reproduce the behavior of the proven bounds on simulated and real data for mapping estimation and domain adaptation on images.

*Both authors contributed equally.

1 Introduction

Optimal Transport (OT) aims at finding the solution of least effort to move mass from one distribution to another. It is a fundamental problem strongly related to physics and has been investigated by mathematicians since the introduction of the problem by Monge [Monge, 1781]. One major result by [Brenier, 1991] proved the existence and derived smoothness properties of optimal transport mapping between continuous distributions.

Optimal Transport in statistical learning. The interest for OT and the related Wasserstein distance have been growing in machine learning in recent years [Arjovsky et al., 2017, Courty et al., 2017b, Frogner et al., 2015] as OT provides a convenient tool to compare the geometry of distributions. In addition, the Wasserstein distance is one of the few divergence that can be applied (and sub-differentiated) on empirical distribution with no need for kernel smoothing as done in MMD [Gretton et al., 2012]. One recent applications of OT concerns the training of Generative Adversarial Networks, a particularly difficult optimization problem where the Wasserstein distance has been used to provide meaningful gradients [Arjovsky et al., 2017, Liu et al., 2018, Lei et al., 2019]. OT has also been used in other learning problems such as unsupervised Domain Adaptation (DA) that aims at training a classifier that perform well on an unlabeled target dataset using information from a related but different labeled source dataset as discussed below in more details.

The rising interest of the machine learning community has been rendered possible thanks to the recent development of efficient optimization techniques. For instance entropic regularization [Cuturi, 2013, Benamou et al., 2015] has lead to new efficient algorithms that can scale to large datasets and even opened the door to stochastic optimization [Genevay et al., 2016, Seguy et al., 2018].

In Machine Learning applications, the distributions are typically unknown and we only have access to finite sample realizations. This raises the question of estimation of the OT mapping between the underlying distributions based only on finite samples. The problem of estimating a continuous mapping has surprisingly received very little attention in the literature. Stavropoulou and Müller [2015] proposed a two-step procedure for estimating a continuous mapping from discrete distributions. Perrot et al. [2016] built up upon this approach by adding ridge-type regularization to prevent overfitting with small samples.

[Fournier and Guillin, 2015, Weed and Bach, 2017] derived the rate of convergence of the empirical distribution to its population counterpart with the Wasserstein distance and showed in particular that these rates suffer from the **curse of dimensionality**. [Hütter and Rigollet, 2019] highlighted that the Monge mapping estimation problem belongs to the class of nonparametric statistical problems that are also known to suffer from the curse of dimensionality. More specifically, they derived a minimax lower bound of the order $O(n^{-1/d})$ where the dimension of the problem d is typically large in modern ML applications. Their result guarantees that OT is hopeless without additional structure assumption. In this paper, we investigate the impact on the estimation rate of

adding structure assumption on OT mapping. We prove that assuming linear OT structure can help **both with statistical and computational performances** as we obtained a practical and easy to compute estimator that attains faster **dimension free parametric rate of estimation** $O(n^{-1/2})$.

Domain adaptation. Domain Adaptation (DA) is a problem in machine learning that is part of the larger Transfer Learning family. The main problem that is addressed in unsupervised DA is how to predict classes on a new (target) dataset that is different from the available (source) training dataset. In order to train a classifier that works well on the target data, we have access to labeled samples (X_i^s, X_i^t) drawn from the source joint feature/target distribution \mathcal{P}_s (whose feature marginal is defined as μ_s) and only to feature samples X_j^t from the marginal μ_t of the joint target distribution \mathcal{P}_t .

The literature on domain adaptation is extensive with numerous different approaches. We will discuss briefly the main approaches before introducing our contribution. A popular approach is based on re-weighting schemes [Sugiyama et al., 2008] where the main idea is to re-weight the samples in order to compensate for the discrepancy between source and target distributions. A classifier can then be estimated by minimizing the weighted source distribution. These approaches have been shown to work very well in numerous cases but a classic failure scenario would be when the distributions do not overlap. Another popular DA approach is known as subspace method. When the datasets are high-dimensional, this approach assumes that there exists a subspace that is discriminant in both source and target domains. This subspace can then be used to train a robust classifier. A standard approach is to minimize the divergences between the two projected distributions onto lower-dimensional spaces [Si et al., 2010]. Source labels (when available) can be integrated into this approach to produce a subspace that preserves the class discrimination after projection [Long et al., 2014]. Finally the last approach aims at aligning the source and target distribution through a more complex representation than linear subspace. Gopalan et al. [2014] proposes to align the distributions by following the geodesic between source and target distributions. Geodesic flow kernel [Gong et al., 2012] aims at adapting distribution using a projection in the Grassmannian manifold and computing kernels using the geodesic flow in this manifold. Note that all the methods above aim at finding a way to compensate for the change in distribution between the source and target domains. The same philosophy has been investigated for neural networks where the feature extraction aims at being indistinguishable between the different domains using Domain Adversarial Neural Network (DANN) [Ganin et al., 2016]. Other approaches have aimed at minimizing the divergence between the distributions in the NN embedded space using covariance matrix alignment (CORAL) [Sun and Saenko, 2016], minimization of the Maximum Mean Discrepancy (MMD) [Tzeng et al., 2017] or Wasserstein distance in the embedded space [Shen et al., 2018]. More references can be found in [Csurka, 2017] about visual adaptation that has been very active recently.

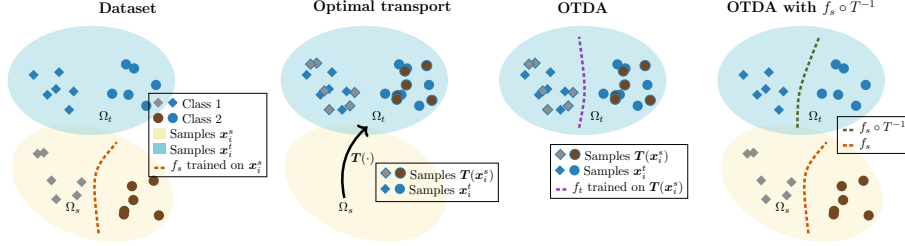


Figure 1: Illustration of Optimal Transport for Domain Adaptation (OTDA) from [Courty et al., 2017b]

Optimal Transport for Domain Adaptation (OTDA). Recently, Courty et al. [2017b] suggested to use OT for Domain Adaptation. This approach assumes that there exists a transformation between the source/target distributions. If this transformation can be accurately estimated, then the knowledge from the source domain can be accurately transferred to the target domain before learning the classifier. While there is in theory several possible mappings between source and target domains, this approach chooses the optimal transport Monge mapping since it corresponds to the least effort (a sound approach often found in nature). This approach has been implemented with success in [Courty et al., 2017b, Perrot et al., 2016, Seguy et al., 2018, Courty et al., 2017a]. Note that as illustrated in Figure 1, target classification can be performed in the source or target domains as discussed in Section 3.

OTDA has also been used in several biomedical applications. Gayraud et al. [2017] have applied OTDA to the problem of P300 detection in Brain Computer Interfaces. It allowed to adapt between different subjects and can potentially decrease the time needed for calibration. OTDA was also applied to the problem of Computer Aided Diagnostic of Prostate cancer from MRI in [Gautheron et al., 2017] to adapt between patients. Finally Chambon et al. [2018] showed that OTDA can improve the performance of sleep stage classification from ElectroEncephaloGrams.

Despite numerous practical applications, little is known about the statistical performances of OTDA approaches. Courty et al. [2017b] and Redko et al. [2017] derived generalization bounds that include a divergence term between the source and target distributions close to that of Ben-David et al. [2010]. Because of this term, those generalization bounds require source and target distributions to be similar in order to achieve domain adaptation. In this paper, we derive explicit generalization bounds for OTDA under milder conditions since OT and its corresponding Monge mapping has the ability to align distributions. The core of our analysis is a new concentration bound for the estimation of Linear Monge mapping between two distributions based on finite samples, which is of interest in itself.

Contributions.

- We prove that adding and exploiting structure assumptions on the OT mapping leads to significant improvements both in terms of statistical bounds and computational complexity. We obtained a dimension-free parametric rate $O(n^{-1/2})$ for the estimation for the OT mapping with a polynomial computational complexity in the dimension d of the problem.
- We derive new generalization bounds for the OTDA problem. Interestingly, these bounds no longer depend on the divergence between the source and target distributions if we assume that there exists a transport map from the source and target distributions.
- We performed numerical experiments on simulated and real datasets that confirm the interest of our approach.

Organization of the paper. The rest of the paper is organized as follows. In Section 2, we focus on the estimation of a linear Monge mapping arising from transport between Gaussian distributions [Takatsu et al., 2011]. We prove that the closed form solution of the linear Monge mapping is also valid for any Borel distributions with finite second order moments. Next, we derive in Theorem 1 our main concentration bound for linear Monge mapping based on finite samples of sub-gaussian distributions. This result is then used in Section 3 to derive a new generalization bound for OT Domain Adaptation. In Section 4, we carry out numerical experiments for the estimation of the monge mapping and the performance of OTDA.

Definitions and notations. In what follows, for any symmetric positive definite matrix B , we denote by $\lambda_{\min}(B)$, $\lambda_{\max}(B)$ the minimum and maximum eigenvalues of B respectively. We also define the effective rank of B by $\mathbf{r}(B) = \frac{\text{tr}(B)}{\lambda_{\max}(B)}$ where $\text{tr}(B)$ is the trace of B . By abuse of notation, $\|\cdot\|$ refers either to the l_2 -norm of a vector or to the operator norm of a matrix. We also define the condition number of B as $\kappa(B) = \frac{\lambda_{\max}(B)}{\lambda_{\min}(B)}$. Finally we use the binary operators \vee and \wedge to denote maximum and minimum respectively.

2 Linear Monge mapping estimation and concentration

Linear Monge mapping between Gaussian distributions Let $\mu_1 = \mathcal{N}(m_1, \Sigma_1)$ and $\mu_2 = \mathcal{N}(m_2, \Sigma_2)$ be two distributions on \mathbb{R}^d . In the remaining we suppose that both Σ_1 and Σ_2 are symmetric positive definite. The Monge mapping for a quadratic loss between μ_1 and μ_2 can be expressed as

$$T(x) = m_2 + A(x - m_1) \quad (1)$$

with

$$A = \Sigma_1^{-\frac{1}{2}} \left(\Sigma_1^{\frac{1}{2}} \Sigma_2 \Sigma_1^{\frac{1}{2}} \right)^{\frac{1}{2}} \Sigma_1^{-\frac{1}{2}} = A^T \quad (2)$$

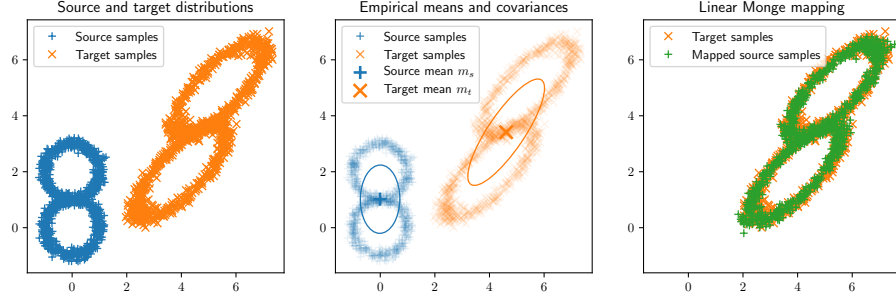


Figure 2: Example of linear Monge mapping estimation between empirical distributions. (left) 2D source and target distributions. (middle) Estimations for means and covariances of the distributions. (right) resulting linear mapping where green samples are the mapped source samples.

This is a well known fact in the Optimal Transport literature [Givens et al., 1984, McCann, 1997, Takatsu et al., 2011, Bhatia et al., 2018, Malagò et al., 2018]. See also [Peyré et al., 2019, Remark 2.31]. Note that the matrix A is actually the matrix geometric mean between Σ_1^{-1} and Σ_2 : $A = \Sigma_1^{-1} \# \Sigma_2$.

Linear Monge mapping between general distributions The linear mapping between Gaussian distribution discussed above is very elegant but real life data in machine learning seldom follow Gaussian distribution (especially classification problems that are at best a mixture of Gaussian). It turns out that the optimal linear transport between arbitrary distributions with finite second order moment is the same as in the Gaussian case. This result was essentially proved in [Dowson and Landau, 1982] where a lower bound on the Fréchet distance between distributions is established. The only missing ingredient was the seminal result on optimal transport that was proved by [Brenier, 1991] several years later. Combining these two results, we obtain Lemma 1 below.

Lemma 1. *Let μ_1 and μ_2 be two Borel probability measures with finite second order moments with expectations m_1, m_2 and positive-definite covariance operators Σ_1, Σ_2 respectively and such that $\mu_2 = T_{\#}\mu_1$ for an affine $\tilde{T}(x) = Bx + c$ with B symmetric positive definite. Then the optimal transport mapping is $\tilde{T} = T$ where T is defined by (1)-(2).*

Estimation bounds for the Monge mapping In practice the distributions μ_1, μ_2 are unknown and we have only access to independent samples $\mathbb{X}_1 = \{X_1^s, \dots, X_{n_1}^s\}$ and $\mathbb{X}_2 = \{X_1^t, \dots, X_{n_2}^t\}$ where the X_i^s are i.i.d. with distribution μ_1 and the X_j^t are i.i.d. with distribution μ_2 . In this case, the linear Monge mapping can be estimated using empirical means and covariances $\hat{m}_1, \hat{m}_2, \hat{\Sigma}_1, \hat{\Sigma}_2$ based on n_1 and n_2 samples respectively. Hence we define the

empirical linear Monge mapping as

$$\hat{T}(x) = \hat{T}_{(\mathbb{X}_s, \mathbb{X}_t)}(x) = \hat{m}_2 + \hat{A}(x - \hat{m}_1), \quad (3)$$

where \hat{A} comes from (2) where the covariances are replaced by their empirical counterpart. Note that this requires $\hat{\Sigma}_1$ to be nonsingular, in other words we need $n_1 \geq d$ observations in the source domain to compute this estimator. An illustration of this method for a highly non-Gaussian distribution can be seen in Figure 2. We can clearly see here that under the assumptions in Lemma 1, we can recover the Monge mapping and align very well complex distributions.

Let T and T' be two mappings, we define the L_2 -divergence between mapped distributions $T_{\#}\mu_1$ and $T'_{\#}\mu_1$ as

$$d(T, T') = \mathbb{E}_{x \sim \mu_1} [\|T(x) - T'(x)\|]. \quad (4)$$

In the next theorem, we prove a bound for the error of estimation of T by \hat{T} .

Theorem 1. *Let μ_1 and μ_2 be sub-Gaussian distributions on \mathbb{R}^d with expectations m_1, m_2 and positive-definite covariance operators Σ_1, Σ_2 respectively. We assume furthermore that*

$$c < \min_{j=1,2} \{(\lambda_{\min}(\Sigma_j))\} \leq \max_{j=1,2} \{\lambda_{\max}(\Sigma_j)\} \leq C, \quad (5)$$

for some fixed absolute constants $0 < c \leq C < \infty$. We also assume that

$$n_1 \geq d, \quad n_2 \geq C' \mathbf{r}(\Sigma_2), \quad (6)$$

for some sufficiently large numerical constant $C' > 0$.

Then, for any $t > 0$, we have with probability at least $1 - e^{-t} - \frac{1}{n_1}$,

$$d(T, \hat{T}) \leq C'' \left(\sqrt{\frac{\mathbf{r}(\Sigma_1)}{n_1}} \vee \sqrt{\frac{\mathbf{r}(\Sigma_2)}{n_2}} \vee \sqrt{\frac{t}{n_1 \wedge n_2}} \vee \frac{t}{n_1 \wedge n_2} \right) \sqrt{\mathbf{r}(\Sigma_1)}, \quad (7)$$

where $C'' > 0$ is a constant independent of $n_1, n_2, \mathbf{r}(\Sigma_1), \mathbf{r}(\Sigma_2), d$.

The detailed proof is provided in Appendix 6.

Comments

- **Statistical performance.** This result is one of the first bound on the quality of an estimated continuous Monge mapping from empirical distribution. By exploiting the additional linear structure of the Monge mapping, we obtain in (1) a faster dimension-free estimation rate of the order $O(n^{-1/2})$ when $n = n_1 = n_2$ which compares favorably to the $O(n^{-\frac{1}{d}})$ obtained with the more general but not computationally feasible estimator in Hütter and Rigollet [2019]. Note that this result also provides a convergence rate for the generalization bound in [Perrot et al., 2016, Eq. (13)] in the linear case where the term $d(T, \hat{T})$ appeared in the bound but was not studied.

- **Computational complexity: general covariance matrices.** The mapping is estimated from empirical distributions by using the empirical version of the means and covariances in (1)-(2). The complexity of estimating those parameters is $O((n_1 + n_2)d^2)$ which is linear *w.r.t.* the number of samples but quadratic in dimensionality d of the data. Eq. (2) also requires the computation of matrix square root and inverse which are $O(d^3)$ leading to a final complexity of $O((n_1 + n_2)d^2 + d^3)$. This complexity scales well with the number of training samples but not with the dimensionality of the space.
- **Computational complexity: convolutional Monge mapping on signals and images.** When the data samples are temporally or spatially stationary signal or images, it is common practice to approximate their Toeplitz or block-Toeplitz covariance matrices by circulant matrices (for large values of dimension d). Indeed, a remarkable property of circulant matrices is that their spectral decomposition can be computed with a Discrete Fourier Transform (DFT): $\Sigma_1 = FD_1F^*$, $\Sigma_2 = FD_2F^*$, Gray [2005]. This is of particular interest because the linear operator in (2) whose computational complexity in the general case is $O(d^3)$ becomes a convolution operator with frequency response $D = D_2^{\frac{1}{2}}D_1^{-\frac{1}{2}}$:

$$A = FDF^* \quad (8)$$

that can be computed efficiently in the Fourier domain using the Fast Fourier transform (FFT) algorithm. Thus this additional assumption leads to a significant speedup of the estimation of the mapping on large dataset and large samples (images or signals). The speedup of the FFT leads to a final computational cost of $O((n_1 + n_2)d \log(d))$ to estimate D that is greatly reduced compared to the general linear case discussed above. Note that in this case in order to use the FFT we suppose that the linear mapping operator is a positive definite circular convolution operator which can introduce artifacts at the border of images.

- **Regularization.** We suppose in all our theoretical results that the covariance matrices are positive definite. In practice this assumption can be false for instance when the data lies in a subspace. A standard practice is to replace the empirical covariance matrices $\hat{\Sigma}_j$ by $\tilde{\Sigma}_j = (1 - \alpha)\hat{\Sigma}_j + \alpha I$ where $\alpha \geq 0$ and I is the identity matrix. In our numerical experiments we did not use this regularization in the simulated examples but needed to use it with $\alpha = 10^{-6}$ on the real life image data.

3 Domain adaptation generalization bound

Now we focus on the problem of domain adaptation where we have access to data from a source joint feature/label distribution \mathcal{P}_s but want to predict well on a target joint distribution \mathcal{P}_t where only features with marginal distribution

μ_t are available. We consider two pairs of samples (X^s, Y^s) and (X^t, Y^t) with values respectively in $\mathcal{X}^s \times \mathcal{Y}$ and $\mathcal{X}^t \times \mathcal{Y}$ with respective joint distributions \mathcal{P}_s and \mathcal{P}_t . Note that \mathcal{X}^s and \mathcal{X}^t are possibly different as it is typically the case in several DA applications.

We define the risk of a prediction rule f in the source domain as

$$R_s(f) := \mathbb{E}_{(X,Y) \sim \mathcal{P}_s} [L(Y, f(X))]. \quad (9)$$

where $(X, Y) \in \mathcal{X}^s \times \mathcal{Y}$ and $L : \mathcal{Y} \times \mathcal{Y} \rightarrow \mathbb{R}^+$ is a Lipschitz loss function *w.r.t.* its second variable. We denote by M_L the Lipschitz constant. For instance we have $M_L = 1$ for the hinge loss. The risk on the target domain $R_t(f)$ is defined similarly with expectation *w.r.t.* \mathcal{P}_t . The optimal prediction rule in the source domain is defined as

$$f_*^s := \operatorname{argmin}_{f: \mathbb{R}^d \rightarrow \mathbb{R}} R_s(f), \quad (10)$$

where the minimization is taken over all measurable functions. We assume here for simplicity that the minimum is attained. Similarly, the optimal prediction rule on target is defined as f_*^t . Note that although the Bayes prediction rule in the previous display does not depends on the marginal distribution of X^s , it is defined on domain \mathcal{X}^s . Therefore, when \mathcal{X}^s and \mathcal{X}^t are different, it is not possible to simply estimate a predictor \hat{f}^s on the source domain \mathcal{X}^s and apply it directly to unlabeled points in the target domain. Courty et al. [2017b] suggested an original approach based on optimal transport to resolve this difficulty.

Optimal Transport Domain Adaptation. Following Courty et al. [2017b], we assume that there exists a mapping m between the source and target such that $\mathcal{P}_t = m_{\#} \mathcal{P}_s$ and that the pushforward m can be expressed as $m(x, y) = (T(x), y)$. In other words the samples in the feature spaces have been transformed by T but have conserved their label through this transformation. This assumption corresponds to a number of real life situations such as a change in the acquisition conditions, sensor drifts, thermal noise in signal processing. This implies that for functions f and g in the source and target domains respectively :

$$R_s(f) = R_t(f \circ T^{-1}) \quad \text{and} \quad R_t(g) = R_s(g \circ T) \quad (11)$$

where T is assumed to be invertible. Note that (11) and (10) imply that the best performance in the source and target domains are equal $R_s(f_*^s) = R_t(f_*^t)$. This motivated the main idea in Courty et al. [2017b] that if one can estimate the mapping T , then it is possible to map the labeled source samples in the target domain with \hat{T} and train a classifier \hat{g} in the target domain using the labels from the original source samples. This classifier can predict the labels for new data in the target domain. In the following we investigate the generalization performance of a similar procedure where we train a classifier \hat{f} in the source domain and use $\hat{f} \circ \hat{T}^{-1}$ to predict in the target domain (see Fig. 1).

We say that the prediction rule f on source domain \mathcal{X}^s is M_f -Lipschitz if $|f(x) - f(y)| \leq M_f \|x - y\|$, for any $x, y \in \mathcal{X}^s$. We can now state a preliminary result.

Proposition 1. *Let f be a M_f -Lipschitz prediction rule in the source domain. Recall that the loss function L is M_L -Lipschitz. Under the OTDA assumption (11), we have*

$$R_t(f \circ \hat{T}^{-1}) \leq R_s(f) + M_f M_L \mathbb{E}_{(X,Y) \sim \mathcal{P}_s} \left[\|\hat{T}^{-1}(T(X)) - \hat{T}^{-1}(\hat{T}(Y))\| \right] \quad (12)$$

If \hat{T} is the linear mapping as defined in (3) then we have

$$R_t(f \circ \hat{T}^{-1}) \leq R_s(f) + M_f M_L \|\hat{A}^{-1}\| d(T, \hat{T}). \quad (13)$$

This result means that our transferred rule $f \circ \hat{T}^{-1}$ will perform almost as well in the target domain as the initial rule f in the source domain up to a remainder term that depends on the estimation error of the transport mapping. Note that (12) is valid for arbitrary transport while (13) is specific to linear Monge mapping.

Generalization bound for finite samples. Note that our goal is to learn a good prediction rule in the target domain $\hat{f}^t : \mathcal{X}^t \rightarrow \mathcal{Y}$ from finite samples. To this end we have access to respectively n_1 and n_2 unlabeled samples from the source and target domains denoted \mathbb{X}_s and \mathbb{X}_t respectively. They will be used to estimate the mapping \hat{T} . We also have access to n_l i.i.d. labeled samples (X_i^l, Y_i^l) , $i = 1, \dots, n_l$ in the source domain $\mathcal{X}^s \times \mathcal{Y}$ independent from \mathbb{X}_s . We illustrate now how to exploit Theorem 1 in the DA prediction problem.

We consider the classification framework in [Mendelson, 2002]. Let \mathcal{H}_K be a reproducing kernel Hilbert space (RKHS) associated with a symmetric nonnegatively definite kernel $K : \mathbb{R}^d \times \mathbb{R}^d \rightarrow \mathbb{R}$ such that for any $x \in \mathbb{R}^d$, $K_x(\cdot) = K(\cdot, x) \in \mathcal{H}_K$ and $f(x) = \langle f, K_x \rangle_{\mathcal{H}_K}$ for all $f \in \mathcal{H}_K$. Assume that $f_* \in \mathcal{H}_K$ and $\|f_*\|_{\mathcal{H}_K} \leq 1$. We consider the following empirical risk minimization estimator:

$$\hat{f}_{n_l} := \operatorname{argmin}_{\|f\|_{\mathcal{H}_K} \leq 1} \frac{1}{n_l} \sum_{i=1}^{n_l} l(Y_i^l, f(X_i^l)). \quad (14)$$

where we assume that the eigenvalues $(\lambda_k)_{k \geq 1}$ of the integral operator T_K of \mathcal{H}_K satisfy $\lambda_k \asymp k^{-2\beta}$ for some $\beta > 1/2$. Let consider for instance Gaussian kernel $K(x, x') = \exp\left(-\frac{\|x-x'\|^2}{\sigma^2}\right)$ with $\sigma > 0$. Then we have, for any $f \in \mathcal{H}_K$, $|f(x) - f(x')| \leq \|f\|_{\mathcal{H}_K} d(x, x')$, with $d^2(x, x') = K(x, x) + K(x', x') - 2K(x, x') = 2 - 2\exp\left(-\frac{\|x-x'\|^2}{\sigma^2}\right) \leq 2\frac{\|x-x'\|^2}{\sigma^2}$. Therefore, this framework guarantees that the predictor \hat{f}_{n_l} is $\sqrt{2}/\sigma$ -Lipschitz continuous. We define the excess risk of a predictor g in the target domain as

$$\mathcal{E}_t(g) = R_t(g) - R_t(f_*^t),$$

where we recall that f_*^t is the Bayes predictor in the target domain. We can now state our main result on OTDA.

Theorem 2. *Let the assumptions of Theorem 1 be satisfied. Assume in addition that $R_s(f_*^s) = R_t(f_*^t)$. Let \hat{T} be the linear mapping as defined in (3). Then we get with probability at least $1 - e^{-t} - \frac{1}{n_1}$,*

$$\begin{aligned} \mathcal{E}_t(\hat{f}_{n_l} \circ \hat{T}^{-1}) &\lesssim n_l^{-2\beta/(1+2\beta)} + \frac{t}{n_l} \\ &+ M_L \left(\sqrt{\frac{\mathbf{r}(\Sigma_2)}{n_2}} \vee \sqrt{\frac{\mathbf{r}(\Sigma_1)}{n_1}} \vee \sqrt{\frac{t}{n_1 \wedge n_2}} \vee \frac{t}{n_1 \wedge n_2} \right) \sqrt{\mathbf{r}(\Sigma_1)}. \end{aligned} \quad (15)$$

The above bound proves that under the mapping assumption, the generalization error of $\hat{f}_{n_l} \circ \hat{T}^{-1}$ converges to the Bayes risk $R_t(f_*^t)$ in the target domain even though we do not have access to any labeled samples in the target domain. This is to the best of our knowledge the first theoretical result that leads to such performances on unsupervised domain adaptation problem. We can get away from the impossibility theorem of domain adaptation of [Ben-David et al., 2010] thanks to the strong assumption on the existence of a linear Monge mapping that allows bypassing the discrepancy between the source and target distributions. Note also that while this result concerns linear Monge mapping, the proof argument can be easily extended to any mapping estimation such as Virtual Regressive training [Perrot and Habrard, 2015] that also have a $o(n^{-1/2})$ convergence rate where n is the number of one-to-one mapping samples between source and target domain. Finally the Lipschitzness of the predictor in the classification problem is satisfied for instance if there is no sample in the vicinity of the decision boundary between classes (margin condition). This Lipschitzness condition can be relaxed to cover more cases especially in the classification problem. We could use for instance the notion of probabilistic Lipschitzness introduced in [Uerner et al., 2011], that is somehow related to the low-noise condition of [Mammen and Tsybakov, 1999].

4 Numerical experiments

In this section we perform numerical experiments to illustrate our theoretical results. The linear mapping estimation from (3) is implemented using the LinearTransport class from the Python Optimal Transport library [Flamary and Courty, 2017]. The convolutional mapping has been implemented with FFT as discussed in section 2.

Note that all the code of the numerical experiments will be made freely available upon publication.

4.1 Convergence of the mapping error and domain adaptation generalization.

Linear mapping error between Gaussian distributions. In these first numerical experiments, we illustrate the convergence speed in term of mapping

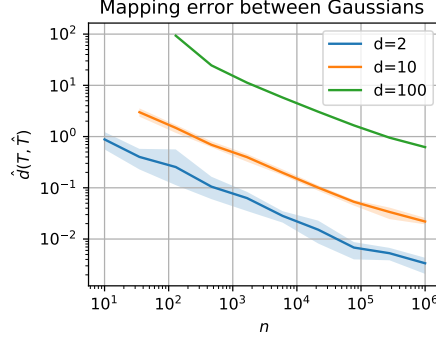


Figure 3: Experiments with Gaussian data. Mapping estimation error as a function of $n = n_1 = n_2$ for different values of d . Colored area corresponds to 10th and 90th percentile.

quality as a function of the number of samples in source and target domains $n = n_1 = n_2$. To this end, for each dimensionality $d \in \{2, 10, 100\}$ we first select the source and target Gaussian distributions by randomly drawing their first and second order moments. For each experiment we randomly draw for $j \in \{1, 2\}$ the means as $m_j \sim \mathcal{N}(\mathbf{0}, 10I_d)$ and the true covariance matrices as $\Sigma_j \sim \mathcal{W}_d(I, d)$ where \mathcal{W}_d denotes Wishart distributions of order d . Once we have selected the population parameters m_i, Σ_i , we generate $n = n_1 = n_2$ i.i.d. samples for each distribution $\mu_j = \mathcal{N}(m_j, \Sigma_j)$. The empirical means and covariances are estimated from those samples and then used to estimate the Monge Mapping $\hat{T}(x)$ in (3).

All experiments are repeated 10 times (Monte Carlo) and the mean mapping error between the true mapping T and the estimated mapping \hat{T} is computed on 10^6 source samples. Figure 3 shows the convergence as a function of n for different values of dimensionality d . This log/log plot clearly shows the slope of $-\frac{1}{2}$ corresponding to the $O(n^{-\frac{1}{2}})$ convergence speed in Theorem 1.

Domain adaptation on simulated examples. In the next experiment we reproduce the domain adaptation bounds obtained in section 3. To this end we design a source classification problem where samples from class + are drawn from $\mathcal{N}(\mathbf{0}, \Sigma_0)$ and samples from class - from $\mathcal{N}(\mathbf{1}, \Sigma_0)$ where $\Sigma_0 \sim \mathcal{W}_d(I, d)$ is drawn and fixed at the beginning of the experiment. The Bayes classifier in this example is known to have a linear separation. Therefore we use a Linear Discriminant Analysis (LDA) classifier to solve this problem. Note that as discussed in section 3 the LDA classifier satisfies the Lipschitz condition since the two class samples are well separated in this experiment. In order to design a domain adaptation problem we generated samples following the source class distributions above and apply a linear mapping $T(x) = Bx + c$ where $B \sim \mathcal{W}_d(I, d)$ is also computed and fixed at the beginning and $c = [10, \dots, 10, 0, \dots, 0]$ with half of its values

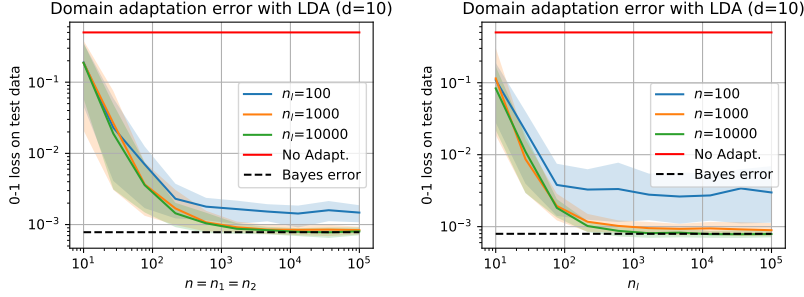


Figure 4: Domain Adaptation experiments with Gaussian data. (left) Domain adaptation test error rate with Gaussian data as a function of n (right) domain adaptation test error rate as a function of n_l . Colored area corresponds to 10th and 90th percentile. We also report the performance of the Bayes classifier on target and the performance if trained on source with no adaptation.

set to 10 and 0 elsewhere. The DA problem above is difficult in the sense that training on source samples with no adaptation leads to bad performances (50% accuracy). It also corresponds to a modeling of real life observation where c can be seen as a sensor drift (here half of them will be uncalibrated between source and target) and the Linear operator B can model a change in the sensor position.

All numerical experiments were performed with $d = 10$. We generate n_l labeled samples in the source domain to train the source classifier f_{n_l} . We also generate $n = n_1 = n_2$ independent unlabeled samples in both source and target to estimate the mapping \hat{T}^{-1} . The DA classifier as suggested by (15) is the function $\hat{f}_{n_l} \circ \hat{T}^{-1}$ and its accuracy evaluated on 10^6 independent target samples. The average classification error rate on 50 Monte Carlo realizations is reported in Figure 4 for different values of n and n_l respectively. We can see in both plots that when both n and n_l become large, the error rate converges to the Bayes error rate $R_t(f_*^t)$.

4.2 Convolutional Monge mapping between images

In this section we investigate the estimation of Monge mapping between images when the mapping is a convolution. To this end we use the well known MNIST dataset [LeCun, 1998] for both 2D filter estimation and convolutional domain adaptation.

Convolutional Domain adaptation Problem. In this section we design a DA problem specific to image data where the transformation between the source and target domain is a convolution operator (which is a special case of linear operator). We design a realistic convolution operator corresponding to a motion blur that is common on images taken in real life conditions Potmesil

and Chakravarty [1983]. The corresponding 2D filter used in the experiment is illustrated in Figure 5 (left). We now apply this blur filter to real images. The source/target datasets are generated as follows. We extract from the MNIST dataset two unlabeled samples sets of equal cardinality $n_1 = n_2 = n$. The first dataset is left unchanged and constitutes the source domain data. The blur filter of Figure 5 is applied to the second dataset that becomes the target domain dataset. The first line in Figure 6 contains the source domain images and the last line the target domain ones.

Estimation of Monge mapping as 2D filters between distributions.

The 2D filters estimated using (8) for a different number of samples n in source/target can be seen in the right part of Figure 5. Note that even for $n = 10$ the filter is surprisingly well estimated considering that there is not even one sample per class in the source/target distributions. For $n = 1000$ the error on the filter is not visible anymore which is also very good for a problem of dimensionality $d = 28 \times 28 = 784$ variables (pixels). Now we estimate our optimal Monge mapping using the source/target domain data and we apply this mapping to an independent sample of MNIST images in the source domain. These mapped images are represented in the center line of Figure 6. We can see that the mapped samples are very similar to the target samples. We also provide a 2D TNSE projection Maaten and Hinton [2008] of the samples before and after mapping in Figure 7. We can see that similarly to the toy data in Figure 2 the mapping aligns the two distributions but also the labels which suggest good domain adaptation performance.

In order to have a quantitative measure of the quality of both linear and convolutional Monge mapping we perform 20 Monte Carlo experiments where we randomly draw a varying number of n samples for estimating the filter described above. The mapping for the linear Monge mapping is estimated using the general formulation in (3) whereas for convolutional mapping, we use the simplified formulation in (8) computed by FFT. The average error of the mapping for both approaches is reported in Figure 8 (left). We can see that the linear mapping has a hard time estimating the mapping especially when $n < d$ (estimated covariance matrix is singular but small regularization is used) but recovers its theoretical convergence speed for $n \geq 10^3$. The convolutional mapping that is much more structured and estimates a smaller number of parameter (block Toeplitz covariance matrix) recovers its theoretical convergence speed for $n \geq 10$.

Convolutional mapping for domain adaptation. We then investigate the performance in domain adaptation between the two domains presented above (from original to filtered MNIST) when training a Convolutional Neural Network (CNN) in the source domain. We use the architecture from the MNIST example of Keras¹ with all hyperparameters fixed for all comparisons. CNN are trained on $n_l = 10^4$ labeled samples and their test error rate is evaluated also on 10^4

¹Available at https://github.com/keras-team/keras/blob/master/examples/mnist_cnn.py

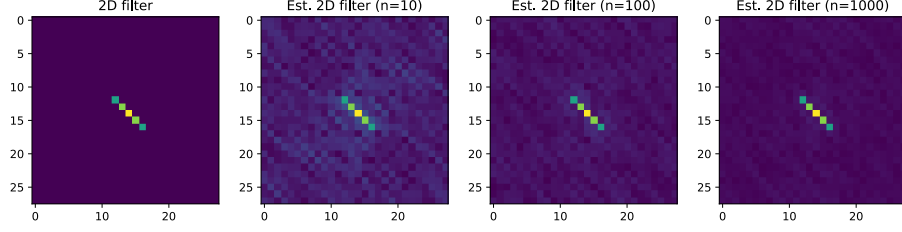


Figure 5: (left) 2D motion blur filter applied to the target MNIST images. (center to right) estimated 2D filters for different number of samples $n = n_1 = n_2$ for the filter estimation. All images are shown with a square root of their magnitude in order to better see small errors.

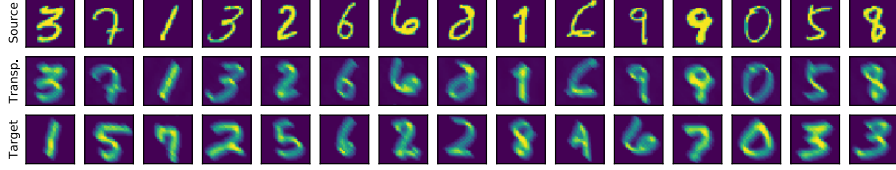


Figure 6: Example images from the MNIST images data. (top) Images from the source distribution. (middle) Examples from the source distribution mapped to the target distribution (convolved with estimated filter). (bottom) Examples from the Target distribution (with the motion blur filter applied).

independent target samples We first compute baselines with a CNN trained on source domain ($\hat{f}_{n_l}^s$) and target domain ($\hat{f}_{n_l}^t$). These baselines will allow us to assess the performance of OTDA classifier $\hat{f}_{n_l}^s \circ \hat{T}^{-1}$ where \hat{T} is estimated using Linear (linear) and Convolutional (conv.) Monge Mapping estimation. The average classification error on test data over 20 Monte Carlo simulations (data sampling) with a varying $n = n_1 = n_2$ is reported in Figure 8 (right). We can see that the convolutional mapping quickly reaches the performance of classifier $\hat{f}_{n_l}^t$ trained directly on target data. This might be due to a regularization effect coming from the convolution operator \hat{T}^{-1} to the data before classification that also seems to lead to a slightly better final performance than $\hat{f}_{n_l}^t$. The linear Monge mapping requires more samples for a proper mapping ($n \geq 10^3$) estimation but also reaches the best performance on target.

5 Conclusion

In this work, we provided the first concentration bound on the quality of a linear Monge mapping when estimated from a discrete sampling. We have shown that this linear mapping can be estimated from non-Gaussian distributions. We discussed the computational complexity of the linear Monge mapping estimation

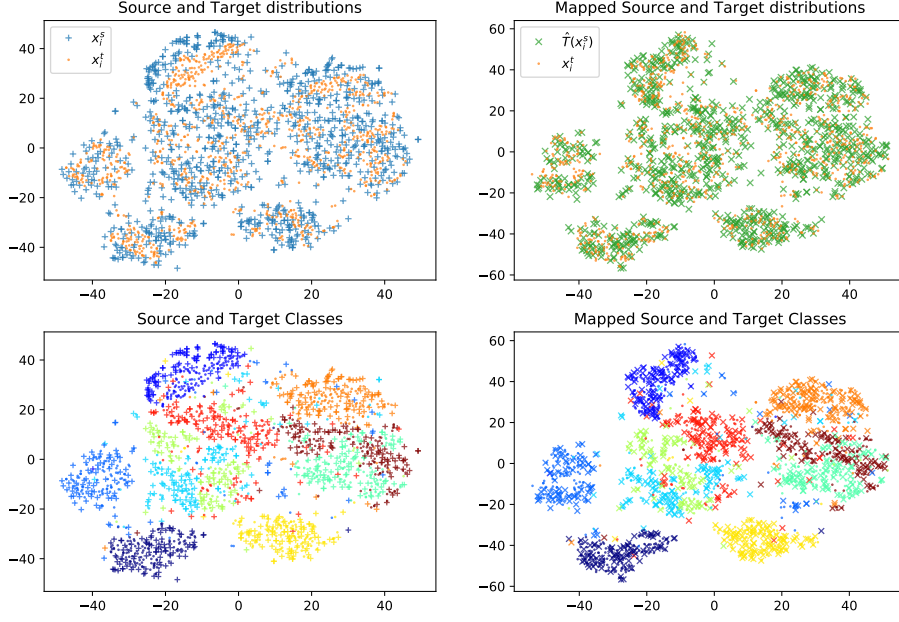


Figure 7: 2D TSNE projection of the MNIST Source, Target and Mapped Source samples. (top line) 2D TSNE projections of Source/Target (left) and Mapped Source/Target (right) colored by distribution. (bottom line) 2D TSNE projections of Source/Target (left) and Mapped Source/Target (right) colored by class.

and investigated a variant that leads to both a speedup and better estimation when the data is a 1D/2D stationary signal which implies a convolutional mapping. This fundamental results allowed us to prove the first bound for Optimal Transport Domain Adaptation [Courty et al., 2017b]. This result states that OT can be used to derive a predictor in the target domain with performance converging to the Bayes risk as the sample size grows. Finally we provided numerical experiments to illustrate the theoretical bounds for both linear and convolutional mapping.

Future works will investigate the design and convergence of an applicable non-linear Monge mapping estimated from finite distributions [Hütter and Rigollet, 2019]. An approach would be to study the quality of the barycentric mapping that has been used in practice [Ferradans et al., 2014, Courty et al., 2017b] and is known to converge weakly to the true Monge mapping [Seguy et al., 2018]. The study of the mapping estimation in the presence of additive noise is also an interesting research direction related to Gaussian deconvolution [Rigollet and Weed, 2018]. Also note that the estimation of a convolutional mapping between distributions of images opens the door for applications in image processing and especially in astronomy where it could be used to estimate changes in the Point Spread Function of a telescope or parameters of weak gravitational

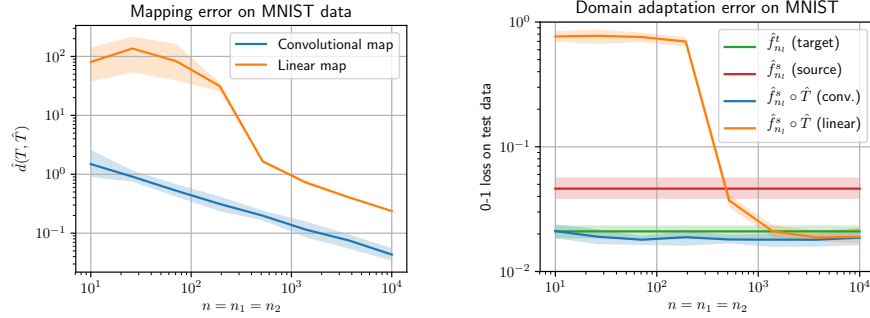


Figure 8: (left) Mapping error on the MNIST data for a convolutional and linear mapping (right) Target prediction error for domain adaptation problem with training on source, training on target and OTDA with linear and convolutional mapping.

lensing [Munshi et al., 2008].

Acknowledgements

The authors want to thank Gabriel Peyré and Nicolas Courty for fruitful discussions about linear Monge mapping and domain adaptation. This work benefited from the support from OATMIL ANR-17-CE23-0012 project of the French National Research Agency (ANR).

References

- M. Arjovsky, S. Chintala, and L. Bottou. Wasserstein generative adversarial networks. In *ICML*, pages 214–223, 2017.
- N. Aronszajn. Theory of reproducing kernels. *Transactions of the American Mathematical Society*, 68:337–404, 1950.
- S. Ben-David, T. Lu, T. Luu, and D. Pál. Impossibility theorems for domain adaptation. In *International Conference on Artificial Intelligence and Statistics*, pages 129–136, 2010.
- J.-D. Benamou, G. Carlier, M. Cuturi, L. Nenna, and G. Peyré. Iterative bregman projections for regularized transportation problems. *SIAM Journal on Scientific Computing*, 37(2):A1111–A1138, 2015.
- R. Bhatia, T. Jain, and Y. Lim. On the bures–wasserstein distance between positive definite matrices. *Expositiones Mathematicae*, 2018.

- Y. Brenier. Polar factorization and monotone rearrangement of vector-valued functions. *Communications on pure and applied mathematics*, 44(4):375–417, 1991.
- S. Chambon, M. N. Galtier, and A. Gramfort. Domain adaptation with optimal transport improves eeg sleep stage classifiers. In *Pattern Recognition in Neuroimaging*, 2018.
- N. Courty, R. Flamary, A. Habrard, and A. Rakotomamonjy. Joint distribution optimal transportation for domain adaptation. In *Advances in Neural Information Processing Systems*, pages 3730–3739, 2017a.
- N. Courty, R. Flamary, D. Tuia, and A. Rakotomamonjy. Optimal transport for domain adaptation. *Pattern Analysis and Machine Intelligence, IEEE Transactions on*, 2017b.
- G. Csurka. Domain adaptation for visual applications: A comprehensive survey. *arXiv preprint arXiv:1702.05374*, 2017.
- M. Cuturi. Sinkhorn distances: Lightspeed computation of optimal transport. In *NIPS*, 2013.
- D. Dowson and B. Landau. The fréchet distance between multivariate normal distributions. *Journal of Multivariate Analysis*, 12(3):450–455, Sept. 1982.
- S. Ferradans, N. Papadakis, G. Peyré, and J.-F. Aujol. Regularized discrete optimal transport. *SIAM Journal on Imaging Sciences*, 7(3):1853–1882, 2014.
- R. Flamary and N. Courty. Pot: Python optimal transport library, 2017.
- N. Fournier and A. Guillin. On the rate of convergence in wasserstein distance of the empirical measure. *Probability Theory and Related Fields*, 162(3-4): 707–738, 2015.
- C. Frogner, C. Zhang, H. Mobahi, M. Araya, and T. Poggio. Learning with a Wasserstein loss. In *NIPS*. 2015.
- Y. Ganin, E. Ustinova, H. Ajakan, P. Germain, H. Larochelle, F. Laviolette, M. Marchand, and V. Lempitsky. Domain-adversarial training of neural networks. *Journal of Machine Learning Research*, 17(59):1–35, 2016.
- L. Gautheron, C. Lartizien, and I. Redko. Domain adaptation using optimal transport: application to prostate cancer mapping. 2017.
- N. T. Gayraud, A. Rakotomamonjy, and M. Clerc. Optimal transport applied to transfer learning for p300 detection. In *7th Graz Brain-Computer Interface Conference 2017*, 2017.
- A. Genevay, M. Cuturi, G. Peyré, and F. Bach. Stochastic optimization for large-scale optimal transport. In *Advances in Neural Information Processing Systems*, pages 3440–3448, 2016.

- C. R. Givens, R. M. Shortt, et al. A class of wasserstein metrics for probability distributions. *The Michigan Mathematical Journal*, 31(2):231–240, 1984.
- B. Gong, Y. Shi, F. Sha, and K. Grauman. Geodesic flow kernel for unsupervised domain adaptation. In *IEEE Conference on Computer Vision and Pattern Recognition (CVPR)*, pages 2066–2073, 2012.
- R. Gopalan, R. Li, and R. Chellappa. Unsupervised adaptation across domain shifts by generating intermediate data representations. *IEEE Transactions on Pattern Analysis and Machine Intelligence*, page To be published, 2014.
- R. M. Gray. Toeplitz and circulant matrices: A review. *Foundations and Trends® in Communications and Information Theory*, 2(3):155–239, 2005.
- A. Gretton, K. M. Borgwardt, M. J. Rasch, B. Schölkopf, and A. Smola. A kernel two-sample test. *Journal of Machine Learning Research*, 13(Mar):723–773, 2012.
- D. Hsu, S. Kakade, and T. Zhang. A tail inequality for quadratic forms of subgaussian random vectors. *Electron. Commun. Probab.*, 17:6 pp., 2012. doi: 10.1214/ECP.v17-2079. URL <https://doi.org/10.1214/ECP.v17-2079>.
- J.-C. Hütter and P. Rigollet. Minimax rates of estimation for smooth optimal transport maps. *arXiv preprint arXiv:1905.05828*, 2019.
- V. Koltchinskii, K. Lounici, et al. Asymptotics and concentration bounds for bilinear forms of spectral projectors of sample covariance. In *Annales de l’Institut Henri Poincaré, Probabilités et Statistiques*, volume 52, pages 1976–2013. Institut Henri Poincaré, 2016.
- Y. LeCun. The mnist database of handwritten digits. <http://yann.lecun.com/exdb/mnist/>, 1998.
- N. Lei, K. Su, L. Cui, S.-T. Yau, and X. D. Gu. A geometric view of optimal transportation and generative model. *Computer Aided Geometric Design*, 68: 1–21, 2019.
- H. Liu, G. Xianfeng, and D. Samaras. A two-step computation of the exact gan wasserstein distance. In *International Conference on Machine Learning*, pages 3165–3174, 2018.
- M. Long, J. Wang, G. Ding, J. Sun, and P. S. Yu. Transfer joint matching for unsupervised domain adaptation. In *Proceedings of the IEEE conference on computer vision and pattern recognition*, pages 1410–1417, 2014.
- L. v. d. Maaten and G. Hinton. Visualizing data using t-sne. *Journal of machine learning research*, 9(Nov):2579–2605, 2008.
- L. Malagò, L. Montrucchio, and G. Pistone. Wasserstein riemannian geometry of gaussian densities. *Information Geometry*, 1(2):137–179, 2018.

- E. Mammen and A. B. Tsybakov. Smooth discrimination analysis. *Ann. Statist.*, 27(6):1808–1829, 12 1999. doi: 10.1214/aos/1017939240. URL <https://doi.org/10.1214/aos/1017939240>.
- R. J. McCann. A convexity principle for interacting gases. *Advances in mathematics*, 128(1):153–179, 1997.
- S. Mendelson. Geometric parameters of kernel machines. In J. Kivinen and R. H. Sloan, editors, *Computational Learning Theory*, pages 29–43, Berlin, Heidelberg, 2002. Springer Berlin Heidelberg. ISBN 978-3-540-45435-9.
- G. Monge. *Mémoire sur la théorie des déblais et des remblais*. De l’Imprimerie Royale, 1781.
- D. Munshi, P. Valageas, L. Van Waerbeke, and A. Heavens. Cosmology with weak lensing surveys. *Physics Reports*, 462(3):67–121, 2008.
- M. Perrot and A. Habrard. Regressive virtual metric learning. In *Advances in Neural Information Processing Systems*, pages 1810–1818, 2015.
- M. Perrot, N. Courty, R. Flamary, and A. Habrard. Mapping estimation for discrete optimal transport. In *Advances in Neural Information Processing Systems*, pages 4197–4205, 2016.
- G. Peyré, M. Cuturi, et al. Computational optimal transport. *Foundations and Trends® in Machine Learning*, 11(5-6):355–607, 2019.
- M. Potmesil and I. Chakravarty. Modeling motion blur in computer-generated images. *ACM SIGGRAPH Computer Graphics*, 17(3):389–399, 1983.
- I. Redko, A. Habrard, and M. Sebban. Theoretical analysis of domain adaptation with optimal transport. In *Joint European Conference on Machine Learning and Knowledge Discovery in Databases*, pages 737–753. Springer, 2017.
- P. Rigollet and J. Weed. Entropic optimal transport is maximum-likelihood deconvolution. *Comptes Rendus Mathématique*, 356(11-12):1228–1235, 2018.
- B. A. Schmitt. Perturbation bounds for matrix square roots and pythagorean sums. *Linear Algebra and its Applications*, 174:215 – 227, 1992. ISSN 0024-3795.
- V. Seguy, B. B. Damodaran, R. Flamary, N. Courty, A. Rolet, and M. Blondel. Large-scale optimal transport and mapping estimation. In *International Conference on Learning Representations (ICLR)*, 2018.
- J. Shen, Y. Qu, W. Zhang, and Y. Yu. Wasserstein distance guided representation learning for domain adaptation. In *Thirty-Second AAAI Conference on Artificial Intelligence*, 2018.

- S. Si, D. Tao, and B. Geng. Bregman divergence-based regularization for transfer subspace learning. *IEEE Transactions on Knowledge and Data Engineering*, 22(7):929–942, July 2010.
- F. Stavropoulou and J. Müller. Parametrization of random vectors in polynomial chaos expansions via optimal transportation. *SIAM Journal on Scientific Computing*, 37(6):A2535–A2557, 2015.
- M. Sugiyama, T. Suzuki, S. Nakajima, H. Kashima, P. von Büna, and M. Kawanabe. Direct importance estimation for covariate shift adaptation. *Annals of the Institute of Statistical Mathematics*, 60(4):699–746, 2008.
- B. Sun and K. Saenko. Deep CORAL: Correlation alignment for deep domain adaptation. In *European Conference on Computer Vision, ECCV*, pages 443–450, 2016.
- A. Takatsu et al. Wasserstein geometry of gaussian measures. *Osaka Journal of Mathematics*, 48(4):1005–1026, 2011.
- E. Tzeng, J. Hoffman, K. Saenko, and T. Darrell. Adversarial discriminative domain adaptation. *CoRR*, abs/1702.05464, 2017. URL <http://arxiv.org/abs/1702.05464>.
- R. Urner, S. Shalev-Shwartz, and S. Ben-David. Access to unlabeled data can speed up prediction time. In *ICML*, 2011.
- C. Villani. *Topics in Optimal Transportation*. American Mathematical Society, Mar. 2003.
- P.-Å. Wedin. Perturbation theory for pseudo-inverses. *BIT Numerical Mathematics*, 13(2):217–232, 1973. doi: 10.1007/BF01933494. URL <https://doi.org/10.1007/BF01933494>.
- J. Weed and F. Bach. Sharp asymptotic and finite-sample rates of convergence of empirical measures in wasserstein distance. *arXiv preprint arXiv:1707.00087*, 2017.

6 Proofs

6.1 Proof of Lemma 1

Proof. The proof is straightforward using e.g. the lower bound on Fréchet distance between two distributions. Let consider a random vector $(x^\top, y^\top)^\top \in \mathbb{R}^{2d}$ with marginal distributions $x \sim \mu_1$ and $y \sim \mu_2$. According to [Dowson and Landau, 1982]:

$$\|m_1 - m_2\|^2 + \text{tr} \left(\Sigma_1 + \Sigma_2 - 2(\Sigma_1 \Sigma_2)^{1/2} \right) \leq \mathbb{E} \|x - y\|^2, \quad (16)$$

with equality if and only if $y \stackrel{d}{=} T(x) = m_2 + A(x - m_1)$ where A is defined as in (2). We now prove that T is a legit transport map. First recall that the Brenier Theorem Brenier [1991] for quadratic loss states that the optimal transport is the unique map T such that $\mu_2 = T_{\#}\mu_1$ and $T = \nabla\varphi$ for some convex function φ , see [Villani, 2003, Theorem 2.32]. Applying Brenier's Theorem with $\varphi(x) = (1/2)x^\top Ax + (m_2 - Am_1)^\top x$ gives the result. \square

6.2 Proof of Theorem 1

From now on, by abuse of notation, $\|\cdot\|$ will refer either to the l_2 -norm of a vector or the operator norm of a matrix.

We first observe that

$$\begin{aligned} \|T(x) - \hat{T}(x)\| &= \|m_2 - \hat{m}_2 + (A - \hat{A})(x - m_1 + \hat{A}(m_1 - \hat{m}_1))\| \\ &\leq \|m_2 - \hat{m}_2\| + \|A - \hat{A}\|\|x - m_1\| + \|\hat{A}\|\|\hat{m}_1 - m_1\|. \end{aligned} \quad (17)$$

6.2.1 Bounding $\|\hat{m}_j - m_j\|$, $j = 1, 2$

Bounding $\|\hat{m}_j - m_j\|$, $j = 1, 2$ poses no particular difficulty. We have $X^s \stackrel{d}{=} \Sigma_1^{1/2} Z$ where $Z \in \mathbb{R}^p$ is a sub-Gaussian random vector, that is, for any deterministic vector α , we have

$$\mathbb{E}[\exp(\langle \alpha, Z_i \rangle)] \leq \exp\left(\frac{\|\alpha\|^2}{2}\right).$$

Note that

$$\hat{m}_1 - m_1 \stackrel{d}{=} \Sigma_1^{1/2} \frac{1}{n_1} \sum_{i=1}^{n_1} Z_i,$$

where Z_1, \dots, Z_{n_1} are independent distributed as Z . Theorem 2.1 in Hsu et al. [2012] gives for any $t > 0$, with probability at least $1 - e^{-t}$,

$$\|\hat{m}_1 - m_1\|^2 \leq \frac{\|\Sigma_1\|}{n_1} \left[\mathbf{r}(\Sigma_1) + 2\sqrt{\mathbf{r}(\Sigma_1)t} + 2t \right] \quad (18)$$

A similar bound holds valid for X^t with Σ_1 and n_1 replaced by Σ_2 and n_2 .

6.2.2 Bounding $\|A - \hat{A}\|$

Matrix geometric mean. We recall first some useful facts. The geometric mean of 2 positive definite matrices is defined as

$$B \# C := B^{1/2}(B^{-1/2}CB^{-1/2})^{1/2}B^{1/2} = B(B^{-1}C)^{1/2}.$$

Note that for readability, in the remaining of this section, the $\#$ operator refers to the matrix geometric mean and not to the pushforward operator $\#$ used in the main paper. The matrix geometric mean satisfies

$$B \# C = C \# B \quad (19)$$

$$(B \# C)^{-1} = B^{-1} \# C^{-1}. \quad (20)$$

We concentrate now on $\|A - \hat{A}\|$ that requires more work. We prove the following result.

Theorem 3. *Let μ_1 and μ_2 be sub-Gaussian distributions with respective means and covariance μ_j, Σ_j , $j = 1, 2$. Assume that*

$$C \left(\sqrt{\frac{\mathbf{r}(\Sigma_1)}{n_1}} \vee \frac{\mathbf{r}(\Sigma_1)}{n_1} \vee \sqrt{\frac{\log(n_1)}{n_1}} \right) \leq \frac{1}{2} \min \left\{ \frac{1}{\kappa(\Sigma_1)}, 1, \frac{\lambda_{\min}(\Sigma_1^{1/2} \Sigma_2 \Sigma_1^{1/2})}{\kappa^{1/2}(\Sigma_1) \|\Sigma_2\|} \right\}, \quad (21)$$

for some sufficiently large numerical constant $C > 0$. Then we have with probability at least $1 - e^{-t} - \frac{1}{n_1}$,

$$\begin{aligned} \|\hat{A} - A\| &\lesssim \frac{\kappa(\Sigma_1) \|\Sigma_2\|}{\lambda_{\min}^{1/2}(\Sigma_1^{1/2} \Sigma_2 \Sigma_1^{1/2})} \left(\sqrt{\frac{\mathbf{r}(\Sigma_2)}{n_2}} \vee \frac{\mathbf{r}(\Sigma_2)}{n_2} \vee \sqrt{\frac{t}{n_2}} \vee \frac{t}{n_2} \right) \\ &\quad + \frac{\kappa(\Sigma_2) \kappa(\Sigma_1) \|\Sigma_2\|}{\lambda_{\min}^{1/2}(\Sigma_2^{-1/2} \Sigma_1 \Sigma_2^{-1/2})} \left(\sqrt{\frac{\mathbf{r}(\Sigma_1)}{n_1}} \vee \frac{\mathbf{r}(\Sigma_1)}{n_1} \vee \sqrt{\frac{\log n_1}{n_1}} \right). \end{aligned} \quad (22)$$

Based on (19)-(20), we deduce that

$$\begin{aligned} \hat{A} - A &= \hat{\Sigma}_1^{-1} \# \hat{\Sigma}_2 - \Sigma_1^{-1} \# \Sigma_2 \\ &= \hat{\Sigma}_1^{-1} \# \hat{\Sigma}_2 - \hat{\Sigma}_1^{-1} \# \Sigma_2 + \hat{\Sigma}_1^{-1} \# \Sigma_2 - \Sigma_1^{-1} \# \Sigma_2 \\ &= \hat{\Sigma}_1^{-1} \# \hat{\Sigma}_2 - \hat{\Sigma}_1^{-1} \# \Sigma_2 + \Sigma_2 \# \hat{\Sigma}_1^{-1} - \Sigma_2 \# \Sigma_1^{-1} \\ &= \hat{\Sigma}_1^{-1} \# \hat{\Sigma}_2 - \hat{\Sigma}_1^{-1} \# \Sigma_2 + (\Sigma_2^{-1} \# \hat{\Sigma}_1)^{-1} - (\Sigma_2^{-1} \# \Sigma_1)^{-1}. \end{aligned} \quad (23)$$

Next we have by definition of the matrix geometric mean that

$$\hat{\Sigma}_1^{-1} \# \hat{\Sigma}_2 - \hat{\Sigma}_1^{-1} \# \Sigma_2 = \hat{\Sigma}_1^{-1/2} \left[(\hat{\Sigma}_1^{1/2} \hat{\Sigma}_2 \hat{\Sigma}_1^{1/2})^{1/2} - (\hat{\Sigma}_1^{1/2} \Sigma_2 \hat{\Sigma}_1^{1/2})^{1/2} \right] \hat{\Sigma}_1^{-1/2}.$$

Taking the operator norm, we get

$$\|\hat{\Sigma}_1^{-1} \# \hat{\Sigma}_2 - \hat{\Sigma}_1^{-1} \# \Sigma_2\| \leq \|\hat{\Sigma}_1^{-1/2}\|^2 \|(\hat{\Sigma}_1^{1/2} \hat{\Sigma}_2 \hat{\Sigma}_1^{1/2})^{1/2} - (\hat{\Sigma}_1^{1/2} \Sigma_2 \hat{\Sigma}_1^{1/2})^{1/2}\|.$$

Perturbation argument. We set $B = \hat{\Sigma}_1^{\frac{1}{2}} \Sigma_2 \hat{\Sigma}_1^{\frac{1}{2}}$ and $\hat{B} = \hat{\Sigma}_1^{\frac{1}{2}} \hat{\Sigma}_2 \hat{\Sigma}_1^{\frac{1}{2}}$. Note that $X = \hat{B}^{1/2} - B^{1/2}$ is solution of $XU + VX = W$, with $U = \hat{B}^{1/2}$, $V = B^{1/2}$, $W = \hat{B} - B$. Then, we can apply Lemma 2.1 in Schmitt [1992] to obtain the following bound:

$$\|X\| \leq \frac{1}{\lambda_{\min}(B^{1/2})} \|\hat{B} - B\|. \quad (24)$$

where $\lambda_{\min}(A)$ is the minimum eigenvalue of symmetric matrix A .

Thus we get

$$\|X\| \leq \frac{1}{\lambda_{\min}(B^{1/2})} \|\hat{\Sigma}_1\| \|\hat{\Sigma}_2 - \Sigma_2\|.$$

Combining the previous display with (24), we deduce that

$$\|\hat{\Sigma}_1^{-1} \# \hat{\Sigma}_2 - \hat{\Sigma}_1^{-1} \# \Sigma_2\| \leq \frac{\kappa(\hat{\Sigma}_1)}{\lambda_{\min}((\hat{\Sigma}_1^{\frac{1}{2}} \Sigma_2 \hat{\Sigma}_1^{\frac{1}{2}})^{1/2})} \|\hat{\Sigma}_2 - \Sigma_2\|, \quad (25)$$

where $\kappa(A) = \|A^{-1}\| \|A\|$ is the condition number of A .

We study now the second difference in the right-hand side of (23). In view of Wedin [1973], we have

$$\|(\Sigma_2^{-1} \# \hat{\Sigma}_1)^{-1} - (\Sigma_2^{-1} \# \Sigma_1)^{-1}\| \leq \|(\Sigma_2^{-1} \# \hat{\Sigma}_1)^{-1}\| \|(\Sigma_2^{-1} \# \Sigma_1)^{-1}\| \|\Sigma_2^{-1} \# \hat{\Sigma}_1 - \Sigma_2^{-1} \# \Sigma_1\|.$$

A similar reasoning to that yielding (25) gives us

$$\|\Sigma_2^{-1} \# \hat{\Sigma}_1 - \Sigma_2^{-1} \# \Sigma_1\| \leq \frac{\kappa(\Sigma_2) \|\Sigma_2 \# \hat{\Sigma}_1^{-1}\| \|\Sigma_2 \# \Sigma_1^{-1}\|}{\lambda_{\min}((\Sigma_2^{-1/2} \Sigma_1 \Sigma_2^{-1/2})^{1/2})} \|\hat{\Sigma}_1 - \Sigma_1\|. \quad (26)$$

Combining the last display with (23) and (25), we obtain

$$\|\hat{A} - A\| \leq \frac{\kappa(\hat{\Sigma}_1)}{\lambda_{\min}^{\frac{1}{2}}(\hat{\Sigma}_1^{\frac{1}{2}} \Sigma_2 \hat{\Sigma}_1^{\frac{1}{2}})} \|E_2\| + \frac{\kappa(\Sigma_2) \|\Sigma_2 \# \hat{\Sigma}_1^{-1}\| \|\Sigma_2 \# \Sigma_1^{-1}\|}{\lambda_{\min}^{\frac{1}{2}}(\Sigma_2^{-1/2} \Sigma_1 \Sigma_2^{-1/2})} \|E_1\|. \quad (27)$$

with $E_1 := \hat{\Sigma}_1 - \Sigma_1$ and $E_2 := \hat{\Sigma}_2 - \Sigma_2$.

We now need to control the following random terms: $\kappa(\hat{\Sigma}_1)$, $\lambda_{\min}((\hat{\Sigma}_1^{\frac{1}{2}} \Sigma_2 \hat{\Sigma}_1^{\frac{1}{2}})^{1/2})$ and $\|\Sigma_2 \# \hat{\Sigma}_1^{-1}\|$. To this end, we introduce the event

$$\mathcal{E}_1 = \left\{ \|\Sigma_1^{-1} E_1\| \leq \frac{1}{2} \right\} \cap \left\{ \|E_1\| \leq \frac{\|\Sigma_1\|}{2} \right\} \cap \left\{ \|E_1\| \leq \frac{\lambda_{\min}(\Sigma_1^{1/2} \Sigma_2 \Sigma_1^{1/2})}{2\sqrt{6} \|\Sigma_2\| \kappa^{1/2}(\Sigma_1)} \right\}. \quad (28)$$

We have on \mathcal{E}_1 that

$$\|\hat{\Sigma}_1^{-1} - \Sigma_1^{-1}\| \leq 2 \|\Sigma_1^{-1} E_1\| \|\Sigma_1^{-1}\|,$$

and consequently

$$\|\hat{\Sigma}_1^{-1}\| \leq 2 \|\Sigma_1^{-1}\|, \quad \|\hat{\Sigma}_1\| \leq \frac{3}{2} \|\Sigma_1\|.$$

Thus we have on \mathcal{E}_1 that

$$\kappa(\hat{\Sigma}_1) \leq 3\kappa(\Sigma_1)$$

and

$$\|\Sigma_2 \# \hat{\Sigma}_1^{-1}\| \leq \|\Sigma_2\|^{1/2} \|\hat{\Sigma}_1^{-1}\|^{1/2} \leq \sqrt{2} \|\Sigma_2\|^{1/2} \|\Sigma_1^{-1}\|^{1/2}.$$

Applying again Lemma 2.1 in Schmitt [1992], we get that

$$\begin{aligned} & \left| \lambda_{\min}((\hat{\Sigma}_1^{1/2} \Sigma_2 \hat{\Sigma}_1^{1/2})^{1/2}) - \lambda_{\min}((\Sigma_1^{1/2} \Sigma_2 \Sigma_1^{1/2})^{1/2}) \right| \\ & \leq \frac{1}{\lambda_{\min}^{1/2}(\Sigma_1^{1/2} \Sigma_2 \Sigma_1^{1/2})} \|\hat{\Sigma}_1^{1/2} \Sigma_2 \hat{\Sigma}_1^{1/2} - \Sigma_1^{1/2} \Sigma_2 \Sigma_1^{1/2}\|. \end{aligned}$$

Next we note that

$$\|\hat{\Sigma}_1^{1/2} \Sigma_2 \hat{\Sigma}_1^{1/2} - \Sigma_1^{1/2} \Sigma_2 \Sigma_1^{1/2}\| \leq 2\|\hat{\Sigma}_1^{1/2} \Sigma_2\| \|\hat{\Sigma}_1^{1/2} - \Sigma_1^{1/2}\|.$$

We apply again Lemma 2.1 in Schmitt [1992] to get

$$\|\hat{\Sigma}_1^{1/2} - \Sigma_1^{1/2}\| \leq \frac{1}{\lambda_{\min}^{1/2}(\Sigma_1)} \|\hat{\Sigma}_1 - \Sigma_1\|.$$

Combining the last three displays, we get on the event \mathcal{E}_1 that

$$\begin{aligned} & \left| \lambda_{\min}((\hat{\Sigma}_1^{1/2} \Sigma_2 \hat{\Sigma}_1^{1/2})^{1/2}) - \lambda_{\min}((\Sigma_1^{1/2} \Sigma_2 \Sigma_1^{1/2})^{1/2}) \right| \\ & \leq \sqrt{6} \frac{\|\Sigma_1\|^{1/2} \|\Sigma_2\|}{\lambda_{\min}^{1/2}(\Sigma_1^{1/2} \Sigma_2 \Sigma_1^{1/2}) \lambda_{\min}^{1/2}(\Sigma_1)} \|E_1\| \\ & \leq \frac{1}{2} \lambda_{\min}((\Sigma_1^{1/2} \Sigma_2 \Sigma_1^{1/2})^{1/2}). \end{aligned}$$

Thus, we get on the event \mathcal{E}_1 that

$$\lambda_{\min}^{1/2}(\hat{\Sigma}_1^{1/2} \Sigma_2 \hat{\Sigma}_1^{1/2}) \geq \frac{1}{2} \lambda_{\min}^{1/2}(\Sigma_1^{1/2} \Sigma_2 \Sigma_1^{1/2}).$$

Combining these facts with (27), we get

$$\|\hat{A} - A\| \lesssim \frac{\kappa(\Sigma_1)}{\lambda_{\min}^{1/2}(\Sigma_1^{1/2} \Sigma_2 \Sigma_1^{1/2})} \|E_2\| + \frac{\kappa(\Sigma_2) \|\Sigma_2\| \|\Sigma_1^{-1}\|}{\lambda_{\min}^{1/2}(\Sigma_2^{-1/2} \Sigma_1 \Sigma_2^{-1/2})} \|E_1\|. \quad (29)$$

Bounding $\|E_1\|$ and $\|E_2\|$. We treat $\|E_1\|$. The result for $\|E_2\|$ follows from the same argument. We set $Y_i = X_i - m_1$, $1 \leq i \leq n$. We have

$$\begin{aligned} \hat{\Sigma}_1 - \Sigma_1 &= \frac{1}{n_1} \sum_{i=1}^{n_1} (X_i - \bar{X})(X_i - \hat{m}_1)^\top \\ &= \frac{1}{n_1} \sum_{i=1}^{n_1} Y_i Y_i^\top - \Sigma_1 - 2(m_1 - \hat{m}_1)(m_1 - \hat{m}_1)^\top. \end{aligned}$$

We get from the previous display

$$\begin{aligned} \|\hat{\Sigma}_1 - \Sigma_1\| &\leq \left\| \frac{1}{n_1} \sum_{i=1}^{n_1} Y_i Y_i^\top - \Sigma_1 \right\| + 2 \|(m_1 - \hat{m}_1)(m_1 - \hat{m}_1)^\top\| \\ &\leq \left\| \frac{1}{n_1} \sum_{i=1}^{n_1} Y_i Y_i^\top - \Sigma_1 \right\| + 2 \|m_1 - \hat{m}_1\|^2. \end{aligned}$$

The second term in the right hand side of the previous display was already treated in (18). We apply now Theorem 2 in Koltchinskii et al. [2016] to handle the first term. We obtain for any $t > 0$, with probability at least $1 - e^{-t}$,

$$\left\| \frac{1}{n_1} \sum_{i=1}^{n_1} Y_i Y_i^\top - \Sigma_1 \right\| \lesssim \|\Sigma_1\| \left(\sqrt{\frac{\mathbf{r}(\Sigma_1)}{n_1}} \vee \frac{\mathbf{r}(\Sigma_1)}{n_1} \vee \sqrt{\frac{t}{n_1}} \vee \frac{t}{n_1} \right).$$

Combining the previous display with (18), we get (up to a rescaling of the constants) for any $t > 0$, with probability at least $1 - e^{-t}$,

$$\|E_1\| \leq C \|\Sigma_1\| \left(\sqrt{\frac{\mathbf{r}(\Sigma_1)}{n_1}} \vee \frac{\mathbf{r}(\Sigma_1)}{n_1} \vee \sqrt{\frac{t}{n_1}} \vee \frac{t}{n_1} \right).$$

for some sufficiently large numerical constant $C > 0$. Taking $t_1 = 2 \log n_1$ and using condition (21), we obtain the result.

Now lets go back to the original problem. We have

$$\|T(x) - \hat{T}(x)\| \leq \|m_2 - \hat{m}_2\| + \|A - \hat{A}\| \|x - m_1\| + \|\hat{A}\| \|\hat{m}_1 - m_1\| \quad (30)$$

Taking the expectation w.r.t. $x \sim \mu_1$, we get

$$\begin{aligned} \mathbb{E}_{x \sim \mu_1} [\|T(x) - \hat{T}(x)\|] &\leq \|m_2 - \hat{m}_2\| + \|A - \hat{A}\| \mathbb{E}_{x \sim \mu_1} [\|x - m_1\|] + \|\hat{A}\| \|\hat{m}_1 - m_1\| \\ &\leq \|m_2 - \hat{m}_2\| + \|A - \hat{A}\| \mathbb{E}_{x \sim \mu_1}^{1/2} [\|x - m_1\|^2] + \|\hat{A}\| \|\hat{m}_1 - m_1\|, \end{aligned} \quad (31)$$

where we use Cauchy-Schwarz's inequality in the last line.

Bounding $\mathbb{E}_{x \sim \mu_1}^{1/2} [\|x - m_1\|^2]$ is a straightforward computation. We get

$$\mathbb{E}_{x \sim \mu_1}^{1/2} [\|x - m_1\|^2] \leq C \|\Sigma_1\|^{1/2} \sqrt{\mathbf{r}(\Sigma_1)},$$

for some numerical constant $C > 0$.

Under conditions (5), (6) with Theorem 3, we get that

$$\|\hat{A}\| \leq_{\mathbb{P}} \|A\| + \|\hat{A} - A\| \leq C$$

for some numerical constant $C > 0$.

Combining (18), Theorem 3 with conditions (5), (6), we get with probability at least $1 - 3e^{-t} - \frac{1}{n_1}$,

$$d(T, \hat{T}) \leq C' \left(\sqrt{\frac{\mathbf{r}(\Sigma_2)}{n_2}} \vee \sqrt{\frac{\mathbf{r}(\Sigma_1)}{n_1}} \vee \sqrt{\frac{t}{n_1 \wedge n_2}} \vee \frac{t}{n_1 \wedge n_2} \right) \sqrt{\mathbf{r}(\Sigma_1)}, \quad (32)$$

for some absolute constant $C' > 0$. Up to a rescaling of the constant, we can replace probability $1 - 3e^{-t} - \frac{1}{n_1}$ by $1 - e^{-t} - \frac{1}{n_1}$.

6.3 Proof of Proposition 1

In view of (11), we have

$$\begin{aligned}
\mathbb{E}_{(x,y) \sim \mathcal{P}_t} [L(y, f \circ \hat{T}^{-1}(x))] &= \mathbb{E}_{(x,y) \sim \mathcal{P}_s} [L(y, f \circ \hat{T}^{-1}(T(x)))] \\
&= \mathbb{E}_{(x,y) \sim \mathcal{P}_s} [L(y, f \circ \hat{T}^{-1}(\hat{T}(x)))] + \mathbb{E}_{(x,y) \sim \mathcal{P}_s} [L(y, f \circ \hat{T}^{-1}(T(x))) - L(y, f \circ \hat{T}^{-1}(\hat{T}(x)))] \\
&\leq \mathbb{E}_{(x,y) \sim \mathcal{P}_s} [L(y, f(x))] + M_f M_L \mathbb{E}_{(x,y) \sim \mathcal{P}_s} [\|\hat{T}^{-1}(T(x)) - \hat{T}^{-1}(\hat{T}(x))\|] \\
&\quad (33)
\end{aligned}$$

$$\begin{aligned}
&\leq \mathbb{E}_{(x,y) \sim \mathcal{P}_s} [L(y, f(x))] + M_f M_L \mathbb{E}_{(x,y) \sim \mathcal{P}_s} [\|\hat{A}^{-1}(T(x) - \hat{T}(x))\|] \\
&\leq R_s(f) + M_f M_L \mathbb{E}_{(x,y) \sim \mathcal{P}_s} [\|\hat{A}^{-1}\| \|T(x) - \hat{T}(x)\|] \\
&\leq R_s(f) + M_f M_L \|\hat{A}^{-1}\| d(T, \hat{T}), \quad (34)
\end{aligned}$$

where the last two lines follows from the definition of \hat{T}^{-1} .

6.4 Proof of theorem 3

Let \mathcal{H}_K be a reproducing kernel Hilbert space (RKHS) associated with a symmetric nonnegatively definite kernel $K : \mathbb{R}^d \times \mathbb{R}^d \rightarrow \mathbb{R}$ such that for any $x \in \mathbb{R}^d$, $K_x(\cdot) = K(\cdot, x) \in \mathcal{H}_K$ and $f(x) = \langle f(x), K_x \rangle_{\mathcal{H}_K}$ for all $f \in \mathcal{H}_K$. See the seminal paper Aronszajn [1950] for more details. Let Π_s be the marginal distribution of X^s and T_K be the integral operator from $L_2(\Pi_s)$ into $L_2(\Pi_s)$ with square integrable kernel K . Then it is known that the operator T_K is compact, self-adjoint and its spectrum is discrete. Let $\{\lambda_k\}_{k \geq 1}$ be the eigenvalues of T_K arranged in decreasing order and $\{\phi_k\}$ are the corresponding $L_2(\Pi_s)$ -orthonormal eigenfunctions. Then the RKHS-norm of any function f in the linear span of $\{\phi_k\}$ can be written as

$$\|f\|_{\mathcal{H}_K}^2 = \sum_{k \geq 1} \frac{|\langle f, \phi_k \rangle_{L_2(\Pi_s)}|^2}{\lambda_k}.$$

Set $f_*^s = \operatorname{argmin}_f R_s(f)$. Assume that $f_* \in \mathcal{H}_K$ and $\|f_*\|_{\mathcal{H}_K} \leq 1$. We consider the following empirical risk minimization estimator:

$$\hat{f}_{n_l} := \operatorname{argmin}_{\|f\|_{\mathcal{H}_K} \leq 1} \frac{1}{n_l} \sum_{i=1}^{n_l} l(Y_i^l, f(X_i^l)). \quad (35)$$

The performances of this procedure have been investigated in Mendelson [2002]. If we assume in particular that $\lambda_k \asymp k^{-2\beta}$ for some $\beta > 1/2$, then there exists a constant $C > 0$ such that with probability at least $1 - e^{-t}$,

$$R_s(\hat{f}_n) \leq R_s(f_*^s) + C \left(n_l^{-2\beta/(1+2\beta)} + \frac{t}{n_l} \right)$$

Under the assumptions of Theorem 1, we have $\|\hat{A}^{-1}\| \leq_{\mathbb{P}} C$ for some numerical constant $C > 0$. Combining the previous display with (34) and Theorem 1, we get with probability at least $1 - e^{-t} - \frac{1}{n_1}$,

$$\begin{aligned}
R_t(\hat{f}_{n_l} \circ \hat{T}^{-1}) - R_s(f_*^s) &\lesssim n_l^{-2\beta/(1+2\beta)} + \frac{t}{n_l} \\
&\quad + M_L \left(\sqrt{\frac{\mathbf{r}(\Sigma_2)}{n_2}} \vee \sqrt{\frac{\mathbf{r}(\Sigma_1)}{n_1}} \vee \sqrt{\frac{t}{n_1 \wedge n_2}} \vee \frac{t}{n_1 \wedge n_2} \right) \sqrt{\mathbf{r}(\Sigma_1)}.
\end{aligned}
\tag{36}$$

The final bound use the fact that with our assumption $R_s(f_*^s) = R_t(f_*^t)$.